Title

Role of Heme Pocket Water in Allosteric Regulation of Ligand Reactivity in Human Hemoglobin

Journal

Biochemistry, 55(29)

ISSN

0006-2960

Authors

Esquerra, Raymond M
Bibi, Bushra M
Tipgunlakant, Pooncharas
et al.

Publication Date

2016-07-26

DOI

10.1021/acs.biochem.6b00081

Peer reviewed

BIOCHEMISTRY
including biophysical chemistry & molecular biology

Article

pubs.acs.org/biochemistry

Role of Heme Pocket Water in Allosteric Regulation of Ligand Reactivity in Human Hemoglobin

Raymond M. Esquerra,[*,†] Bushra M. Bibi,[†] Pooncharas Tipgunlakant,[†] Ivan Birukou,[‡,∥] Jayashree Soman,[‡] John S. Olson,[‡] David S. Kliger,[§] and Robert A. Goldbeck[*,§]

[†]Department of Chemistry and Biochemistry, San Francisco State University, San Francisco, California 94132, United States

[‡]Department of Biochemistry and Cell Biology and W. M. Keck Center for Computational Biology, Rice University, Houston, Texas 77005, United States

[§]Department of Chemistry and Biochemistry, University of California, Santa Cruz, California 95064, United States

ABSTRACT: Water molecules can enter the heme pockets of unliganded myoglobins and hemoglobins, hydrogen bond with the distal histidine, and introduce steric barriers to ligand binding. The spectrokinetics of photodissociated CO complexes of human hemoglobin and its isolated α and β chains were analyzed for the effect of heme hydration on ligand rebinding. A strong coupling was observed between heme hydration and quaternary state. This coupling may contribute significantly to the 20−60-fold difference between the R- and T-state bimolecular CO binding rate constants and thus to the modulation of ligand reactivity that is the hallmark of hemoglobin allostery. Heme hydration proceeded over the course of several kinetic phases in the tetramer, including the R to T quaternary transition. An initial 150 ns hydration phase increased the R-state distal pocket water occupancy, n_w(R), to a level similar to that of the isolated α (∼60%) and β (∼10%) chains, resulting in a modest barrier to ligand binding. A subsequent phase, concurrent with the first step of the R → T transition, further increased the level of heme hydration, increasing the barrier. The final phase, concurrent with the final step of the allosteric transition, brought the water occupancy of the T-state tetramer, n_w(T), even higher and close to full occupancy in both the α and β subunits (∼90%). This hydration level could present an even larger barrier to ligand binding and contribute significantly to the lower iron reactivity of the T state toward CO.

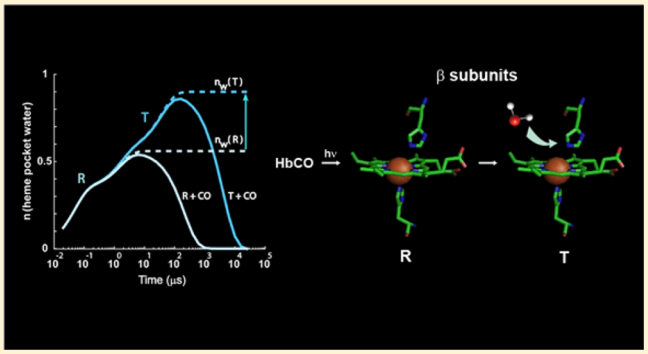

Hydration by a single water molecule can markedly affect the function of heme protein active sites, as has been observed in the binding of small gaseous molecules to the oxygen storage protein myoglobin. A water molecule localized near the binding site of the myoglobin heme pocket presents a substantial steric barrier to ligand binding. The free energy required to displace this water (which is hydrogen bonded to the distal histidine residue but not coordinated to the ferrous heme iron atom) lowers bimolecular ligand binding rate constants by a factor of ∼10 relative to those of variants lacking distal water.[1,2] The polarity of the distal histidine residue drives the high occupancy of distal pocket water (DPW) and concomitant blocking of ligand access in wild-type myoglobin. The hydrogen bonding potential of the distal histidine also provides a mechanism for preferentially stabilizing bound O_2 and reducing its rate of dissociation up to 1000-fold.[3−5]

Structural studies detect a water molecule hydrogen bonded to the distal histidine residue in the α chains of the oxygen transport protein hemoglobin,[6] suggesting that water plays a role in modulating ligand binding in the Hb tetramer similar to that observed in myoglobin.[7] This idea is supported by spectrokinetic evidence obtained from R-state hemoglobin and isolated hemoglobin chains showing that the DPW occupancy of the α chains presents a significant steric barrier to ligand binding at the heme site.[5,8] Similarly, the low ligand affinity of the human hemoglobin variant Hb Chico has been attributed to enhanced DPW occupancy in β subunits,[9] and noncoordinated DPW has been found to be a primary factor controlling ligand access in bacterial truncated hemoglobins.[10,11]

Internal water molecules are present in most globular proteins,[12] where they exchange with bulk water solvent on the time scale of 0.1−10 μs.[13] X-ray crystallographic or nuclear magnetic resonance (NMR) methods are typically used to determine the occupancies of water molecules in internal protein cavities.[12,13] However, positional disorder may obscure the electron densities of internal waters in X-ray diffraction studies, and orientational disorder and short residence times may similarly limit NMR detection.[1,14−17] Thus, the extent to which water may be buried in the internal cavities of proteins has remained an open question, although computational modeling may be helpful in this regard.[16,18]

Received: February 2, 2016
Revised: May 6, 2016
Published: June 29, 2016

DOI: 10.1021/acs.biochem.6b00081
Biochemistry 2016, 55, 4005−4017

We have recently developed a spectrokinetic method for detecting noncoordinated water in the distal heme pocket of pentacoordinate ferrous heme proteins.[19] A small spectral shift in the heme visible absorption bands that accompanies the entry of water can be used to detect the speed and extent to which water takes up residence in the distal pocket near the heme after photodissociation of the carbon monoxide complex.[8,17,19,20] Water occupancies measured in this way were used to disentangle the contributions of steric blockade by water, the geminate rebinding yield (which is determined by the intrinsic Fe−CO bond formation and escape rates for ligands in the heme pocket), and ligand diffusion rates to the observed CO binding rate constants for a series of Mb mutants representing different distal pocket polarities.[19] Modulation of the water occupancy was found to be a critical factor by which distal pocket residue mutations affected ligand binding rate constants in the variants studied. The rate at which water enters the Mb pocket is limited by the time scale of ligand escape, ∼0.5 μs.[17,19,21] As expected from the steric constraint imposed by the size of the distal cavity, water entry does not precede ligand escape in wild-type Mb or any variant studied to date.

Distal pocket water occupancy may vary with quaternary structure in the hemoglobin tetramer, a possibility that could affect ligand reactivity. It is well-known that ligand binding affinities and rate constants are coupled to the quaternary states, labeled R (high affinity) and T (low affinity) in two-state models.[22] The classical explanation for these changes, as described by Perutz, Karplus, and others, links structural changes at the $\alpha_1\beta_2$ subunit interface, such as salt bridge formation, to tensions communicated via the F helix to the proximal histidine residue and its iron−imidazole coordination bond to the heme moiety within each subunit.[23,24] These forces pull the heme iron atom out of the plane of the porphyrin ring and away from the distal binding site in the T state, lowering the affinity of the pentacoordinate heme for a sixth ligand.

The sensitivity of association rate constants and affinities of small gaseous ligands such as O_2 and CO to DPW occupancy in heme proteins noted above leads to the following question: Could tertiary structural changes at the heme sites associated with R−T allostery also alter the distal pocket water occupancy and thus provide an additional mechanism for modulating ligand reactivity? Hydration of the Hb tetramer's surface and central cavity is coupled to quaternary structure. The tetramer loses ∼60 surface-bound water molecules overall in the R → T transition, after first picking up ∼10 additional water molecules in passing through the allosteric transition state.[25,26] However, the coupling of quaternary structure to hydration changes internal to the protein remains an open question.[27] This issue is addressed in the study presented here by using spectrokinetic techniques that monitor the entry of water into the distal pockets of the hemoglobin tetramer after CO photodissociation triggers protein structural relaxation from the R to the T quaternary state.

The structural and kinetic complexity of the Hb tetramer makes quantitative assays of heme pocket hydration more challenging than in monomeric globins such as myoglobin. In particular, the deoxyheme band spectral changes accompanying tertiary and quaternary structural relaxations after HbCO photodissociation tend to obscure the spectrokinetic signal for heme hydration. However, a reexamination of the simpler kinetics of the isolated HbCO chains provided a key to unraveling some of this complexity by providing model spectra that have allowed us to deconvolute and identify the separate contributions of water entry and protein structural relaxation in the tetramer.

We find that water takes up residence in the distal pocket in several stages. The early stages increase DPW occupancy in the subunits to levels similar to those observed in the R-like isolated α chains. However, additional water is then observed to enter the pocket as the protein relaxes from the R to the T quaternary state, revealing that distal pocket hydration is coupled to hemoglobin allostery. The additional impediment to ligand access imposed by increased DPW occupancy appears to be great enough to contribute significantly to the low reactivity of T-state hemoglobin toward CO, particularly in β subunits.

MATERIALS AND METHODS

Preparation of the Hb Tetramer and Isolated Chains. Isolated Hb α and β chains were prepared from native human Hb tetramers by the method of Parkhurst and Parkhurst, as modified by Birukou et al.[5,28] Mutant Hb α and β chains were prepared as described by Birukou et al.[5] HbA tetramers were prepared for laser photolysis experiments at a concentration of 100−120 μM in pH 7.3, 100 mM sodium phosphate buffer with sodium dithionite (250 μM) under 1 atm of CO in a 4 mm × 1 cm sealed quartz cuvette.[17,20,29] The Hb-chain samples were prepared similarly except that the concentrations ranged from 10 to 100 μM and cuvette path lengths ranged from 1 to 10 cm. The protein concentrations were varied over these ranges to ensure that the signals measured did not include contributions from chain homodimers and homotetramers. However, the postphotolysis kinetics showed no dependence on heme concentration for the isolated subunits. Static absorption spectra of samples measured before and after the laser photolysis protocol were also identical, indicating no oxidation during the experiments. The sample temperature was held at 20 ± 0.1 °C by a thermoelectric system (TLC50, Quantum Northwest, Liberty Lake, WA).

Time-Resolved Spectroscopy. Time-resolved absorption data were measured as described previously using a broadband xenon flashlamp probe, multichannel detection, and frequency-doubled Nd:YAG laser actinic pulses (8 ns, 40 mJ).[17,20,29] Photolysis difference spectra were recorded over the visible band spectral region (500−650 nm) at 41 time delays spaced logarithmically from 20 ns to 20 ms after the laser pulse. Each time-delayed spectrum represented the average of ∼1000 photolysis measurements.

Singular Value Decomposition Analysis. A singular value decomposition (SVD) analysis was applied to the matrix of time-resolved multiwavelength absorption data, **A**, for CO photodissociation experiments for each species studied. These analyses yielded the decomposition $\mathbf{A} = \mathbf{U}\cdot\mathbf{S}\cdot\mathbf{V}^{\mathrm{T}}$, where orthonormal spectral and temporal basis vectors were contained in the columns of matrices **U** and **V**, respectively, and the contribution weights of the basis vectors, the singular values, were contained in diagonal matrix **S**.[30,31] Our analysis focused on the two largest SVD components of **A**, $U_1S(1,1)V_1^{\mathrm{T}}$ and $U_2S(2,2)V_2^{\mathrm{T}}$. In general, SVD components do not correspond to particular physicochemical processes. However, an approximate correspondence is more likely when processes are both spectrally and temporally distinct, as is observed in CO photolysis data for the myoglobin visible absorption bands.[8,19] The first SVD component is similar in spectral shape (U_1) to the CO-unbound minus CO-bound heme difference spectrum, and its temporal vector approximately represents the time courses for geminate first-order and bimolecular CO rebinding

DOI: 10.1021/acs.biochem.6b00081
Biochemistry 2016, 55, 4005−4017

processes. The second component corresponds spectrally to a blue shift in the CO-unbound heme spectrum (U_2), and its temporal vector approximately represents the process of entry of water into the distal pocket (concurrent with escape of geminate ligand from the distal heme pocket) and exit (concurrent with bimolecular rebinding).

Global Kinetic Fitting. We further applied a phenomenological fitting procedure to identify kinetic intermediates in the spectrokinetic data matrices obtained for the HbCO chains and tetramer. Data for each species were fit globally over all wavelengths simultaneously to a matrix equation representing parallel first-order decays: **A** = **B**·**C**, where **B** contained the decay-associated spectra (*b*-spectra) and **C** contained exponential decay functions.[31,32] The advantage of this phenomenological approach is that, unlike SVD basis spectra, *b*-spectra are typically constrained to represent first-order or pseudo-first-order physicochemical processes. In particular, *b*-spectra represent the difference spectra between intermediates in the case of a kinetic mechanism containing sequential first-order rate processes with well-separated decay time constants. This condition was approximately met in the results for HbCO chains and tetramers that are reported below.

Deconvolution of *b*-Spectra. The *b*-spectra obtained for the HbCO tetramer were further analyzed to estimate the individual contributions of physicochemical processes that may be convoluted by the complexity of the tetramer kinetic mechanism into one observed rate process in the phenomenological fitting procedure. A least-squares solution for the (overdetermined) coefficients of the deconvolution matrix equation **B** = **M**·**d** was obtained from **d** = pinv(**M**)·**B**, where pinv is the Moore−Penrose pseudoinverse, **B** is the matrix of tetramer *b*-spectra (wavelength × process index), **M** is the matrix of model spectra (wavelength × model spectrum index), and **d** is the vector of deconvolution coefficients. Three model spectra were used in the deconvolution procedure. Model spectra for distal pocket water entry and protein tertiary structural relaxation were obtained from the *b*-spectra measured for isolated α chains (after adjusting for the different concentrations of the initial deoxy or unliganded heme produced in the tetramer and isolated-chain photolysis experiments, and then dividing by the geminate ligand escape yield of the isolated α chains). For the third model spectrum, representing CO rebinding in the absence of DPW, we used the *b*-spectrum for the fastest geminate rebinding process observed in the HbCO tetramer (labeled phase I below). Finally, a baseline offset was used as a fourth component in the procedure to account for small absorption baseline differences ($\leq$1%) between spectra measured in the Hb α-chain and tetramer photolysis experiments.

RESULTS

Distal Pocket Hydration of Isolated Hemoglobin Chains. Photolysis difference spectra were measured for isolated HbCO α and β chains in the heme visible bands (see Figures 1 and 2) to monitor the entry of water into the distal heme pockets. Although the slightly larger geminate yield of the β chains is evident, in other respects the spectrokinetics of the chains appear at first sight to be similar in the figures. To detect the subtle spectral changes indicating water entry, we applied a signal analysis technique, SVD, to the data, the results of which are shown in Figure 3. The first SVD component for each of the species shown was similar in spectral shape and time course (Figure 3, red traces) to the deoxy−CO difference

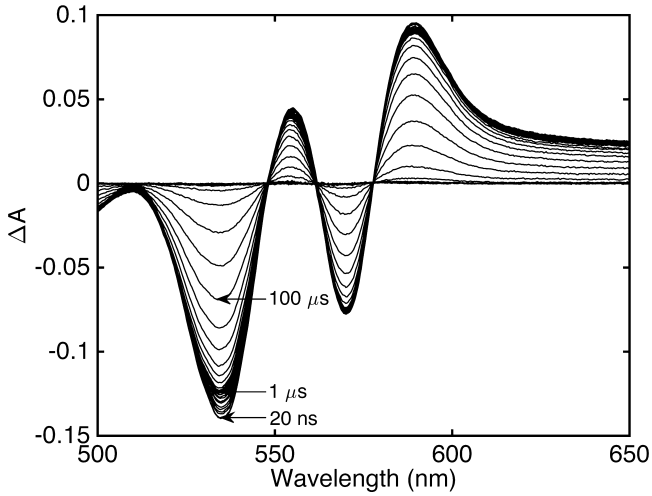

Figure 1. Visible band time-resolved photolysis difference spectra of isolated HbCO α chains at 20 °C. Spectra were measured at logarithmically distributed time delays: 18 time delays covering the range from 20 ns to 1 μs and 25 covering the range from 1.6 μs to 40 ms. Each time-delayed spectrum represented the average of ∼1000 photolysis measurements.

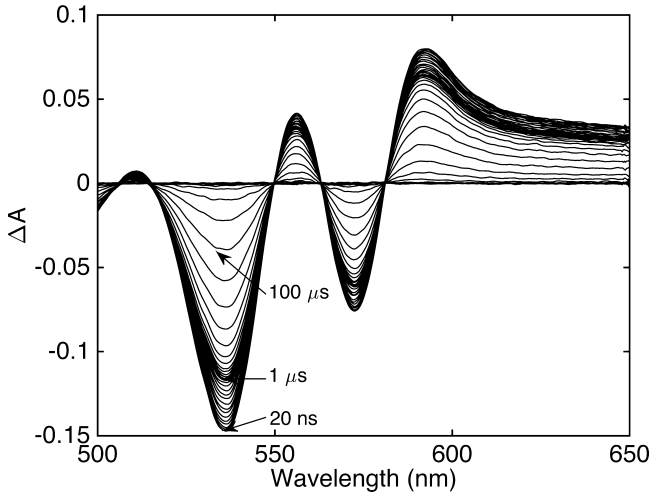

Figure 2. Visible band time-resolved photolysis difference spectra of isolated HbCO β chains at 20 °C. Time delays are as described in the legend of Figure 1.

spectrum familiar from many previous Mb- and Hb-chain photolysis studies. The second SVD component for the isolated Hb α chains (panels b and g, blue traces) was roughly similar in spectral shape and amplitude to the water entry signal identified previously in MbCO photolysis experiments (panels a and f). The second SVD component is smaller in amplitude than the first by a factor of ∼20 in these high-DPW occupancy species, reflecting the subtle effect that the presence of the DPW molecule has on the deoxy heme absorption band. The amplitude of the corresponding signal for the β chains is much smaller (panels c and h) than that observed in Mb or Hb α chains, indicating that less water entered the distal pocket after CO photodissociation. The α-chain DPW occupancy is 0.6, a significant barrier to ligand rebinding, whereas water occupancy is too small to play a significant role in β-chain rebinding kinetics.[8] We applied the spectral deconvolution procedure discussed below for the Hb tetramer (see Materials and

DOI: 10.1021/acs.biochem.6b00081
Biochemistry 2016, 55, 4005−4017

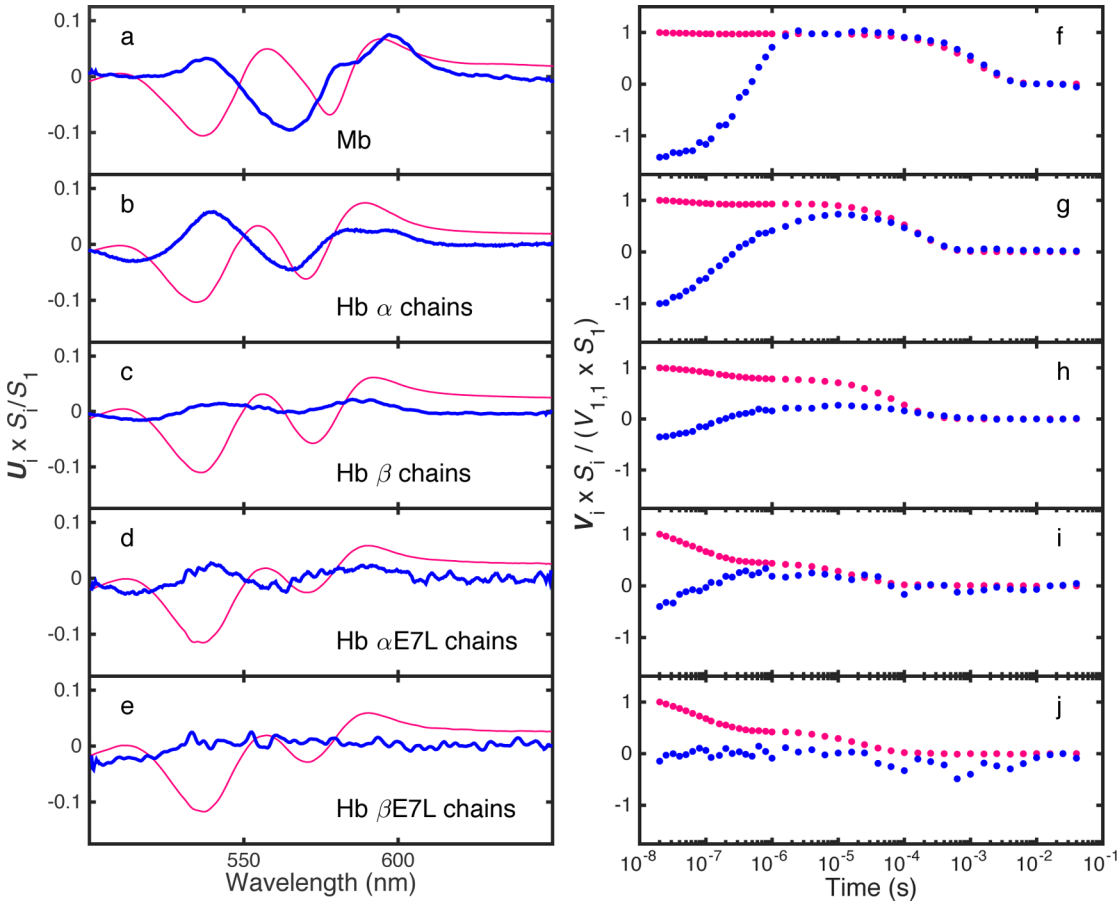

Figure 3. First two SVD components of CO photolysis TROA spectra in the visible bands of isolated Hb chains at 20 °C: (a and f) Mb (shown for comparison), (b and g) Hb α chains, (c and h) Hb β chains, (d and i) Hb αE7L chains, and (e and j) Hb βE7L chains. Panels a–e: (red) first spectral basis vector and (blue) second spectral vector, scaled by their singular values as indicated by the *y*-axis label. The second spectral vectors were multiplied by a factor of 20 for the sake of clarity. Panels f–i: (red) first temporal basis vector and (blue) second temporal basis vector, scaled by their singular values as indicated by the *y*-axis label. The second temporal basis vectors were multiplied by a factor of 25 for the sake of clarity.

Methods) to the isolated β-chain data and determined an upper limit on DPW occupancy of ~0.1.

Control experiments for DPW occupancy were also performed on isolated hemoglobin chains in which the distal histidine (E7) residue was replaced with an apolar leucine residue. As expected, the magnitudes of the second SVD components of the LeuE7 mutants of both chain types were markedly reduced compared with those of the respective wild-type chains (Figure 3, panels d, e, i, and j), indicating little or no water entry after CO photodissociation. This observation was consistent with the trend we observed previously in photolyzed MbCO E7 mutants, wherein the Leu mutant had a DPW occupancy that was negligible compared with that of the wild-type protein and no electron density for distal pocket water was observed in the crystal structure of LeuE7 deoxyMb.[19]

The time courses of the first SVD components, $\mathbf{V}_1$, of visible band TROA data for the noncooperative, monomeric species are shown in panels f–j of Figure 3 and generally show a submicrosecond geminate CO rebinding phase and a microsecond to millisecond bimolecular rebinding phase. The temporal vector of the second SVD component, $\mathbf{V}_2$, was established in previous work on wild-type myoglobin and its distal pocket variants as mainly reflecting the time course of a small blue shifting (~1 nm) of the deoxy absorption band caused by the entry of a DPW molecule.[19] The entry of water into the distal pocket of myoglobin is rate-limited by the geminate escape of CO ligand from the pocket. However, in contrast to the situation observed in myoglobin, the $\mathbf{V}_2$ vector for the isolated Hb α chains (Figure 3g) displayed both an initial phase that evolved after the nanosecond geminate rebinding phase seen in $\mathbf{V}_1$ and a second slower phase.

The observation of a slower evolution in the $\mathbf{V}_2$ vector for the α chains suggested that, unlike the kinetics observed in myoglobin, water entry might not be rate-limited exclusively by the relatively rapid escape of CO from the isolated chains seen in the geminate phase, the kinetics of the latter reflecting both ligand rebinding and movement out of the distal pocket. To explore this possibility further, we applied a model-free fitting procedure that fit the matrix of spectrokinetic data to multiple first-order decays, optimizing the exponential decay time constants over all wavelengths simultaneously. The results of this global kinetic analysis for the Hb α-chain photolysis data are presented in Figure 4. These data were best fit with four exponential decays, representing first-order (or pseudo-first-order) rate processes for (1) geminate CO rebinding, (2) distal pocket water entry, (3) protein structural relaxation, and (4) bimolecular CO rebinding. The earliest process, geminate CO rebinding and escape, proceeded significantly faster than water entry did. The temporal separation of the two processes allowed us to obtain a direct measurement of the intrinsic rate constant for the entry of water into the heme pocket of a ferrous heme protein ($k_w = 6 \times 10^6$ s^{-1}). This value is the same

DOI: 10.1021/acs.biochem.6b00081
Biochemistry 2016, 55, 4005–4017

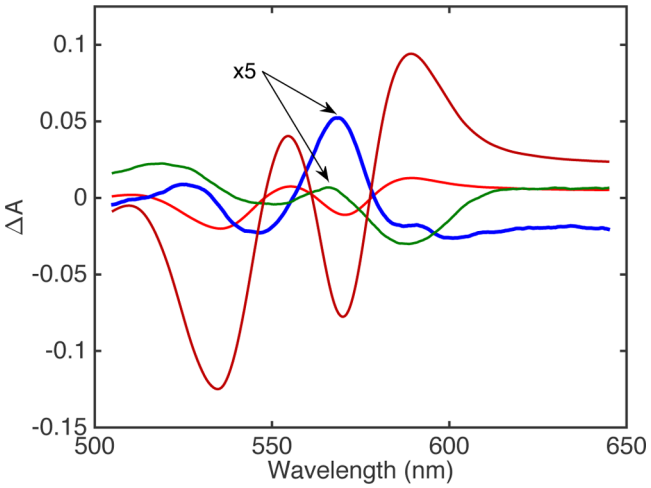

Figure 4. *b*-Spectra (decay spectra) for the four-exponential fit to ligand photolysis of isolated HbCO α chains: (red) geminate CO rebinding, (blue) distal pocket water entry, (green) protein structural relaxation, and (dark red) bimolecular CO rebinding. Exponential lifetimes and relative spectral amplitudes are listed in Table . Spectra for water entry and protein structural relaxation are shown multiplied by a factor of 5 for the sake of visibility.

as the rate constant reported previously by Esquerra et al. for this system and that measured by Cao et al. for the entry and binding of a water molecule to ferric heme in metMb.[8,33]

The main feature of the α-chain *b*-spectrum for water entry (Figure 4, blue line), which represented a dry−wet deoxy pocket difference spectrum, was a bisignate band shape centered near the deoxy band maximum at 555 nm. This band shape corresponded to an ∼1 nm blue shift of the heme deoxy absorption band upon entry of water into the distal pocket. The green line in Figure 4 shows the band shape determined for a process occurring at ∼2 μs that we assigned to protein structural relaxation. The kinetics of the latter process were similar to those reported previously for structural relaxation in the isolated chains,[34] and its band shape agrees reasonably well with the larger absorbance changes that accompany tertiary structural relaxations at the heme pocket after ligand photolysis in the tetramer.[35,36]

As discussed in the next section, the α-chain *b*-spectra determined here provided important keys for the analysis of the time-resolved multiwavelength absorbance data for the Hb tetramer. By providing model spectra for water entry and R to T-like tertiary structural relaxations, these results allowed us to estimate the individual contributions of these processes to the kinetics of the tetramer, despite their expected overlap in time and in optical absorbance data with those for CO rebinding.

Distal Pocket Hydration of the Hemoglobin Tetramer. The visible band TROA data for the human hemoglobin tetramer (see Figure 5) show, in addition to a bimolecular CO rebinding phase to the R state on the time scale of hundreds of microseconds, a slower rebinding process on the millisecond time scale, representing binding of CO to those tetramers that underwent quaternary structural relaxation to the T state. A global kinetic analysis that fit exponential decay functions to the tetramer TROA data yielded the *b*-spectra shown in Figure 6. We used six exponential time constants as free parameters in the fitting procedure to facilitate assignment of the rate processes observed here, our assignments being based on the results of previous six-exponential analyses of TROA data for

Table 1. Isolated HbCO α-Chain Lifetimes (τ) and Relative Spectral Amplitudes of the Four Kinetic Phases Observed after Photolysis, Geminate CO Rebinding (Gem), Distal Pocket Water Entry (DPW), Protein Structural Relaxation, and Bimolecular Rebinding (Hb+CO) (*b*-spectra shown in Figure 4)[a]

	Gem	DPW	protein relaxation	Hb+CO	total
τ	70 ns	180 ns	1.8 μs	170 μs	–
amplitude	0.12	0.06	0.04	0.78	1.00

[a]Spectral amplitudes were calculated as the vector norms of *b*-spectra and normalized to a total amplitude of unity.

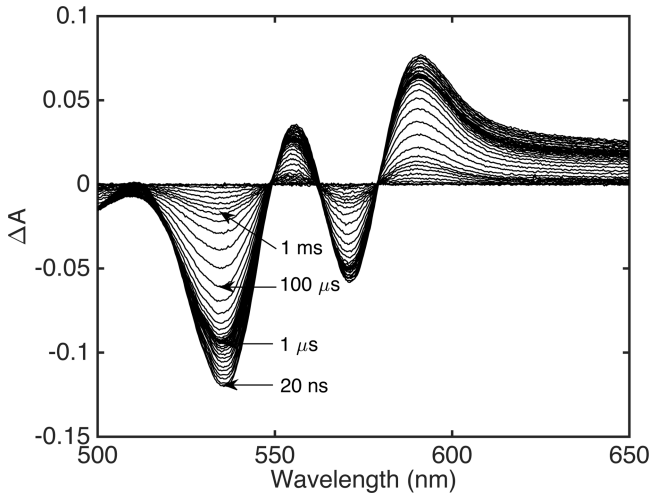

Figure 5. Visible band time-resolved photolysis difference spectra of the HbCO tetramer. Time delays are as described in the legend of Figure 1.

the Soret band spectral region of HbCO.[29,37,38] The time constants obtained from the visible band TROA data were in good agreement with those determined from the Soret band measurements. The first two kinetic phases (labeled I and II in Scheme 1) corresponded mainly to nanosecond geminate CO rebinding, which appears to be best described in hemoglobin as a biexponential process.[39] The geminate phases were concurrent with tertiary structural relaxation at the unliganded heme sites, as they relax from the liganded tertiary conformation found in prephotolysis HbCO, labeled r″, to an intermediate conformation, r′, along the pathway to the equilibrium deoxy heme conformation, r, of the R-state tetramer (we use lowercase r and t to refer to the high- and low-ligand affinity tertiary conformations, respectively, of deoxy hemes within a tetramer). The third phase (III), with a time constant of ∼2 μs, corresponded mainly to protein structural relaxations. These relaxations comprised the completion of tertiary relaxation at the heme sites to their equilibrium unliganded conformations within the R quaternary structure (represented as $[\mathrm{Fe}\cdots]_{\mathrm{Rr}'} \rightarrow [\mathrm{Fe}\cdots]_{\mathrm{Rr}}$ in Scheme 1) and, notably, the alteration of $\alpha_1\beta_2$ and $\alpha_2\beta_1$ dimer−dimer contacts and relative rotation of the $\alpha_1\beta_1$ and $\alpha_2\beta_2$ dimers that represent the major steps in a compound R → T pathway ($[\mathrm{Fe}\cdots]_{\mathrm{Rr}'} \rightarrow [\mathrm{Fe}\cdots]_{\mathrm{T}'\mathrm{r}}$).[37,40−44] Phase III appears to produce two populations of tetramers: (1) those that have undergone most of the large scale quaternary structural change along the RT pathway and are thus committed to completing the R → T transition (T′r) and (2) those remaining in the R quaternary state (Rr). Because the rate of quaternary change depends on the ligation

DOI: 10.1021/acs.biochem.6b00081
Biochemistry 2016, 55, 4005−4017

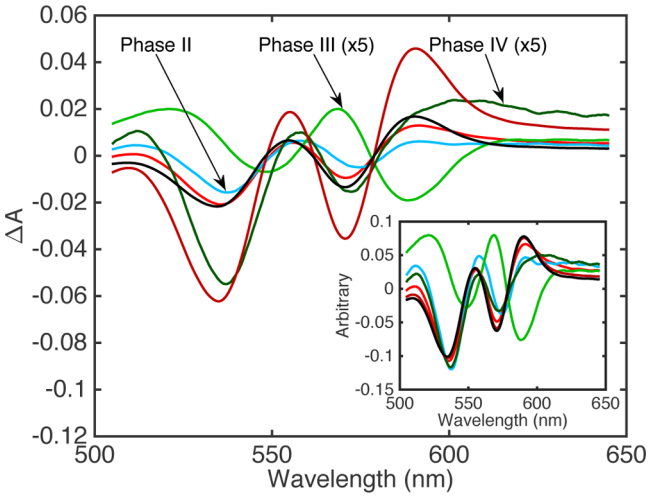

Figure 6. Visible band *b*-spectra (exponential decay spectra) for ligand photolysis of the human HbCO tetramer. The same spectra are shown in the inset normalized by their vector norms to better compare band shapes. The six observed kinetic phases (and their nominal assignments) in order of increasing lifetime (lifetimes and relative amplitudes listed in Table) are (1) (red) phase I (first CO geminate rebinding), (2) (light blue) phase II (second geminate rebinding), (3) (light green) phase III (initial R → T relaxation), (4) (dark green) phase IV (final R → T relaxation, competes with R_0 + CO bimolecular recombination), (5) (dark red) phase V (bimolecular rebinding to R-state tetramers), and (6) (black) phase VI (bimolecular rebinding to T-state tetramers). Nominal assignments were taken from previous multiwavelength TROA studies.[37,39−41] Spectra for phases III and IV are shown multiplied by a factor of 5 for the sake of visibility. Deviations of the band shapes (see the inset) for phases II−IV from those for pure CO rebinding (phase I) and/or R to T relaxation (green trace in Figure 4) indicate the presence of an additional process, distal pocket water entry, as was most evident for phase II.

state of the tetramer, the population of T′r tetramers was probably drawn mainly from those tetramers that remained fully unliganded after the geminate rebinding phases, i.e., from the $Rr'_0 \rightarrow T'r_0$ process. The quaternary structural transition was then completed in a second step (phase IV), with a lifetime that fell within the range traditionally assigned to one-step kinetic models of the R → T transition (20−40 μs). More precisely, the latter process corresponded mainly to the $T'r_0 \rightarrow Tt_0$ transition, the final quaternary and tertiary structural relaxations leading to the equilibrium T state. At this stage, the quaternary structural changes initiated in phase III and completed in phase IV are communicated back to the heme sites. This relaxation process competes with bimolecular rebinding ($T'r_0$ + CO → Rr_1).[37] The presence of this kinetic branching between structural relaxation and ligand rebinding processes ∼40 μs after photolysis accounts for the mixing, evident in Figure 6, of the CO rebinding band shape into the *b*-spectrum assigned to phase IV. Finally, CO recombined with the bulk of R-state tetramers (phase V) with a bimolecular rate constant (4.8×10^6 M^{-1} s^{-1}) that was ∼20 times faster than that observed (2.5×10^5 M^{-1} s^{-1}) for rebinding to the smaller population of T-state tetramers (phase VI) produced by quaternary structural relaxation.

The *b*-spectra for phases II−IV stood out as deviating from the CO rebinding band shape that dominated the other *b*-spectra (I, V, and VI) as shown in the inset of Figure 6. This result was not surprising in the cases of the *b*-spectra for phases III and IV (light and dark green traces, respectively), which reflected structural changes at the heme site concomitant with R to T relaxation. However, the deviation of the *b*-spectrum for phase II (light blue trace) from that of phase I suggested that the spectrum for phase II contained contributions from both distal pocket water entry and structural relaxation band shapes shown in Figure 4 for isolated α subunits, in addition to the signal for internal CO rebinding. In other words, both distal pocket water entry and protein structural relaxation were proceeding roughly concurrently with what was originally labeled as the second geminate rebinding process. This scenario seems reasonable given (1) the similarity of the phase II lifetime (150 ns) to the time constant for water entry observed in the α chains (180 ns) and (2) the detection in previous hemoglobin studies of tertiary protein structural relaxations on time scales of <1 μs.[45]

Spectral Deconvolution of Heme Hydration, Structural Relaxation, and Ligand Rebinding in Hb Tetramers. To investigate the individual contributions of water entry and structural relaxation processes to the Hb tetramer *b*-spectra, we applied a deconvolution procedure (see Materials and Methods) that used the water entry and protein relaxation band shapes obtained from the isolated α chains, along with the

Scheme 1

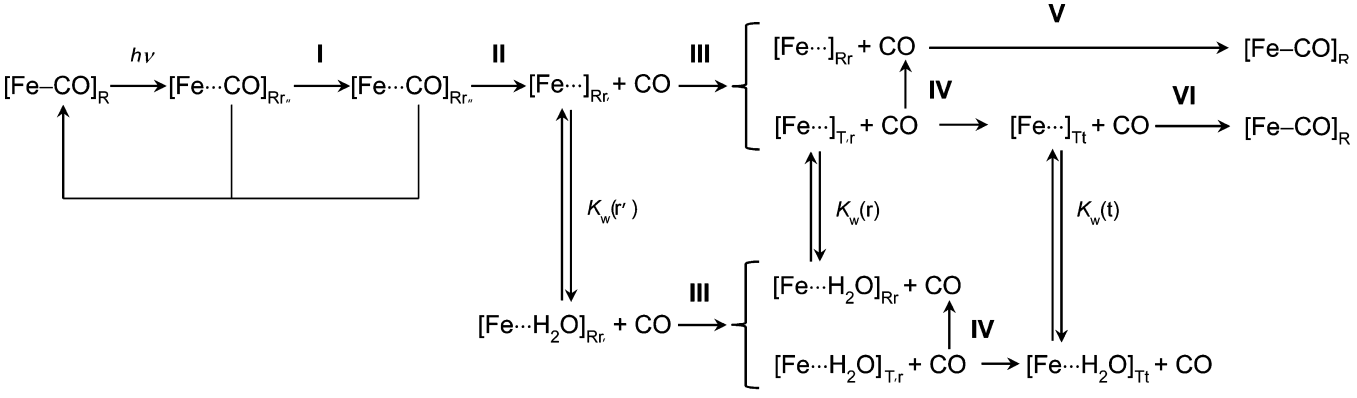

$$K_w(r') < K_w(r) < K_w(t), K_w = n_w/(1 - n_w)$$

DOI: 10.1021/acs.biochem.6b00081
Biochemistry 2016, 55, 4005−4017

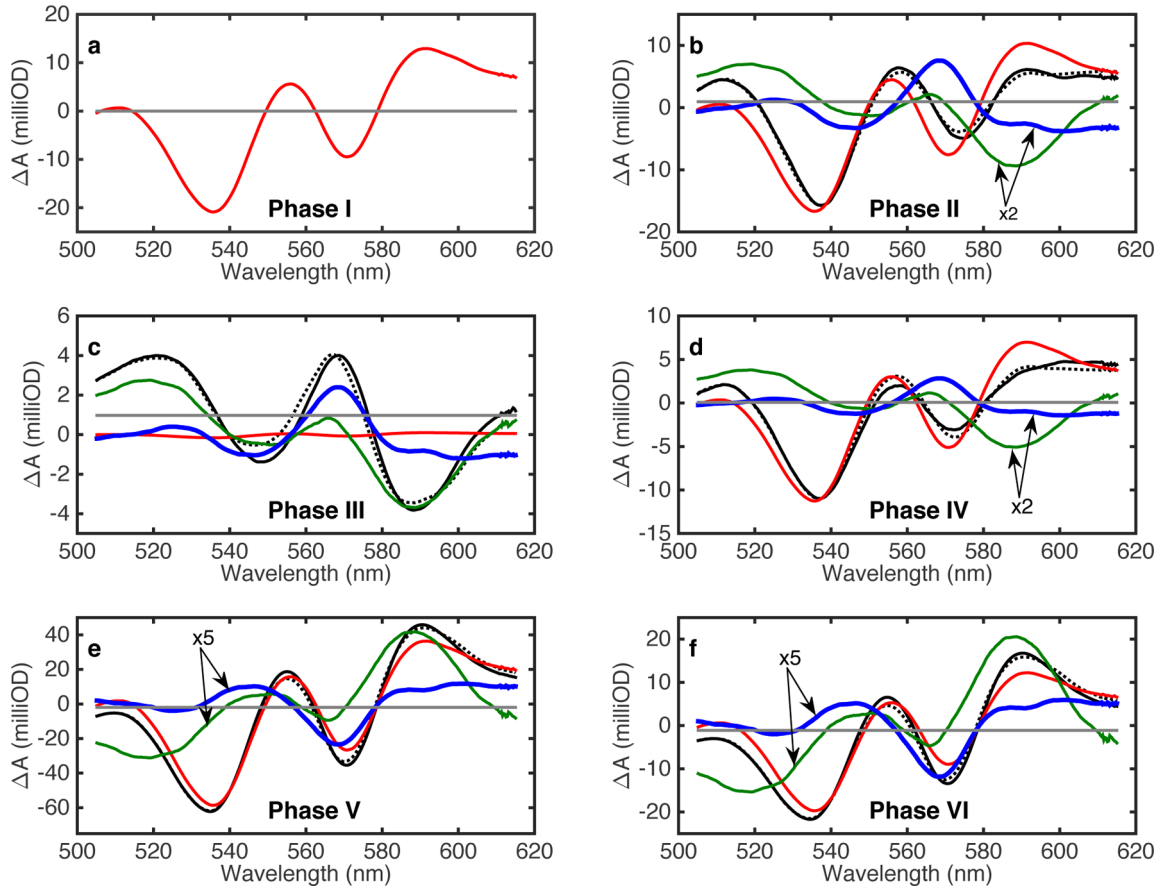

Figure 7. Deconvolution of (black) *b*-spectra for kinetic phases I–VI (a–f, respectively) into components for (red) CO rebinding, (green) protein structural relaxation, (blue) distal pocket water entry, and (gray) baseline offset. The water entry and structural relaxation components are multiplied by the factors indicated in panels b and d–f for the sake of clarity. The sum of the deconvoluted spectral components (dotted line) is shown for comparison with the measured *b*-spectrum for each kinetic phase. The amplitudes of the deconvoluted components were used to calculate the corresponding component values listed in Table 2, as described in the text. Note that the signs of the water entry and protein relaxation signals are reversed in panels e and f from those shown in panels b–d, consistent with the loss of DP water and reversal of protein relaxation expected when bimolecular CO rebinding returns the protein to its prephotolysis state (see the text and Table 2).

Table 2. HbCO Tetramer Lifetimes (τ), Relative Amplitudes, and Calculated CO Rebinding (Δn_{CO}), Distal Pocket Water Entry (Δn_w), and Protein Structural Relaxation Components for the Six Kinetic Phases (Scheme 1) Observed after Photolysis (*b*-spectra and nominal assignments shown in Figure 6)

	I	II	III	IV	V	VI	total
τ	48 ns	150 ns	1.6 μs	38 μs	210 μs	4.0 ms	–
spectral amplitude[a]	0.15	0.10	0.04	0.07	0.47	0.17	1.00
Δn_{CO}[b]	0.16	0.13	0.001	0.088	0.46	0.16	1.00
relaxation[c]	0.0	0.80	0.62	0.43	−1.42	−0.70	−0.27
Δn_w[d]	0.0	0.22	0.14	0.083	−0.28	−0.14	0.033
baseline offset[e]	0.0	0.005	0.005	0.000	−0.010	−0.006	–

[a]Spectral amplitudes were calculated as the vector norms of *b*-spectra and normalized to a total amplitude of unity. [b]Deconvoluted Δn_{CO} values were normalized to unity for total recombination assuming complete photolysis. [c]Deconvoluted relaxation component values were normalized to the protein relaxation signal observed in the isolated α-chain experiments (after adjusting for small differences in the per heme concentrations and CO photolysis levels between the tetramer and isolated-chain experiments). The phase I value was zero by construction. [d]Deconvoluted DPW component values were normalized to the per deoxy heme water signal observed in the isolated α-chain experiments (after adjusting for small differences in the per heme concentrations and prompt CO photolysis levels between the tetramer and isolated-chain experiments) and multiplied by the n_w value of isolated α chains,[8] 0.6, to obtain per (total) heme water occupancy values for the tetramer. The phase I value was zero by construction. [e]Absorption offsets optimized in the deconvolution procedure, normalized to the maximal peak–trough difference of the photolysis difference spectra (Figure 5).

band shape for CO rebinding (phase I *b*-spectrum), as model spectra (500–615 nm spectral region). This approach recognized that the phenomenological kinetic phases shown in Scheme 1 represented a simplification of the complex dynamical processes underlying the evolution of heme ligation, tertiary and quaternary structure, and distal pocket hydration observed after photolysis of the HbCO tetramer. Thus, the *b*-spectra associated with the six kinetic phases each represented a

DOI: 10.1021/acs.biochem.6b00081
Biochemistry 2016, 55, 4005–4017

convolution of the distinct spectral signatures for ligand binding, structural relaxation, and water entry or exit. The deconvolution of the *b*-spectra into these spectral components is shown in Figure 7. By deconvoluting the contributions of model spectra for the three underlying processes to each of the *b*-spectra, we were able to obtain the amplitude values for water entry, protein structural relaxation, and CO rebinding listed in Table 2. Determining the water entry values required knowing the DPW occupancy of the isolated α chains, for which we used a value of 0.6.[8]

The deconvoluted CO rebinding values for kinetic phases I, II, V, and VI were in reasonable agreement with spectral amplitudes calculated directly from the *b*-spectra vector norms, reflecting the dominant contribution that CO rebinding made to the spectral amplitudes of those phases. A more stringent test of the deconvolution procedure was presented by the sums of the protein structural relaxation and the DPW components over all kinetic phases. The sum of the positive structural relaxation component spectra for phases II−IV is expected to be canceled by the sum of the negative values associated with the return to the prephotolysis R state during late time CO rebinding phases V and VI. Similarly, the sum of the positive DPW entry component values for phases II−IV is expected to equal the loss of DPW during the late time CO rebinding phases. Cancellation of the positive- and negative-signal kinetic phase sums was observed to hold for both the DPW and relaxation amplitudes within errors of 7 and 15%, respectively (Table 2). This result represents a reasonably good agreement with expectations given the simplicity of the modeling procedure and the kinetic complexity of the hemoglobin tetramer. The greatest challenge to the precision of the deconvolution procedure occurs for kinetic phases V and VI, in which the final displacement of distal water and the reversal of photolysis-induced structural relaxations represented small signals set against the strong background signal of CO recombination.

The distal pocket water entry values for the HbCO tetramer show the prompt entry of water on the submicrosecond time scale, as observed in MbCO and in isolated Hb α chains. Normalizing the phase II Δn_w value (Table 2) to the overall geminate escape yield gives a value for the DPW occupancy of 0.3 on a per deoxy heme basis. If, for the moment, we assume negligible β-chain occupancy, this would further imply an α-chain n_w value of 0.6, the value observed for the isolated chains. However, a new feature observed in the tetramer was the additional entry of water in later, microsecond time scale stages associated with allosteric transition phases III and IV. Stages II−IV are shown in Scheme 1 as producing intermediates with successively increasing values of K_w, the equilibrium constant for hydrogen bonding of a water molecule from the bulk solvent with the distal histidine. These later hydration stages roughly doubled the amount of water apparent in the deoxy pockets, averaged over chain type and quaternary state, resulting in a level of heme hydration significantly greater than that expected from the isolated-chain observations.

Water Occupancies of Deoxy Heme Sites. The spectrokinetic results presented above indicate that, after complete photolysis of the CO complex, water entered the deoxy heme sites of the R-state Hb tetramer in several kinetic phases, some of which were concurrent with the R to T quaternary structural transition. The Δn_w values for phases III and IV indicate an additional fractional increase in water occupancy in going from the Rr to Tt conformational states of the subunits. In principle, the Δn_w values in Table 2 can be used to estimate n_w values for the unliganded hemes in each quaternary state. However, note that the Δn_w values presented in Table 2 were on a per photolyzed heme basis, normalized to the prompt yield of photolyzed heme (i.e., before geminate and bimolecular ligand recombination), whereas the quantity we were interested in determining, n_w, represents the water occupancy of only those hemes that remain unliganded at any given stage in the postphotolysis kinetics, i.e., occupancy on a per deoxy heme basis. Therefore, we used the Δn_{CO} (fractional CO rebinding) values in Table 2 to estimate the fraction of initially photolyzed hemes remaining unliganded at a given stage in the kinetics. The Δn_w value for a given kinetic phase was divided by this fraction to estimate the corresponding value of n_w for the deoxyhemes at the different stages of ligand rebinding after photolysis. The general procedure based on this approach for summing water entry values to obtain the deoxy heme water occupancy after the *k*th kinetic phase can be expressed as

$$n_w(k) = \sum_{i=1}^{k} \{\Delta n_w(i) / \sum_{j=1}^{i} [1 - \Delta n_{CO}(j)]\} \quad (1)$$

We obtained estimates of n_w for each quaternary state from the data in Table 2 by two different routes. First, we followed the procedure described above (eq 1), summing the water entry values for phases II and III and dividing by the fractional yield of deoxy hemes remaining after geminate recombination (0.70), to obtain an estimate of n_w of 0.52 for the R state. Second, we also used an alternative approach that simply looked at the amount of DPW lost during R-state bimolecular CO rebinding to obtain a more direct estimate for the R-state n_w value: we divided the absolute value of the Δn_w value for DP water displacement during phase V by the fraction of hemes undergoing this displacement (0.46), which yielded a value of 0.60. The mean of these two independently determined n_w(R) values was 0.56. Similarly, we obtained our first estimate of n_w for the T state by applying eq 1. We started with the first n_w value obtained above for the R state and added to that the Δn_w value observed for phase IV, divided by the fraction of hemes that undergo the transition from the R to T quaternary state. The latter quantity was given by the fraction of hemes observed to undergo the T-state bimolecular recombination phase (VI), 0.16. This procedure yielded an estimate of n_w of ≈1 for the T state, the theoretical maximum. A second, more direct estimate of DPW occupancy in the T state was obtained by dividing the absolute value of the Δn_w value observed for DP water displacement during phase VI T-state CO rebinding by the fraction of hemes undergoing that reaction, which yielded an n_w value of 0.88. Thus, both estimates of n_w(T) indicate values that are significantly greater than n_w(R), which is on the order of 0.5−0.6.

We estimated the uncertainty in the Δn_w values in Table 2 to be ∼10% by considering several equalities that these values should satisfy in the model. These were the equality of (1) the two independently derived values for n_w(R), (2) the two independently derived values for n_w(T), and (3) the sum of the incoming (positive) Δn_w values and the absolute value of the sum of the outgoing (negative) Δn_w values. The equalities between these quantities were satisfied with errors of 11, 11, and 7%, respectively, which led to our given estimate. We note that the spectral deconvolution procedure itself was quite stable with respect to spectral noise. We found that injection into the

DOI: 10.1021/acs.biochem.6b00081
Biochemistry 2016, 55, 4005−4017

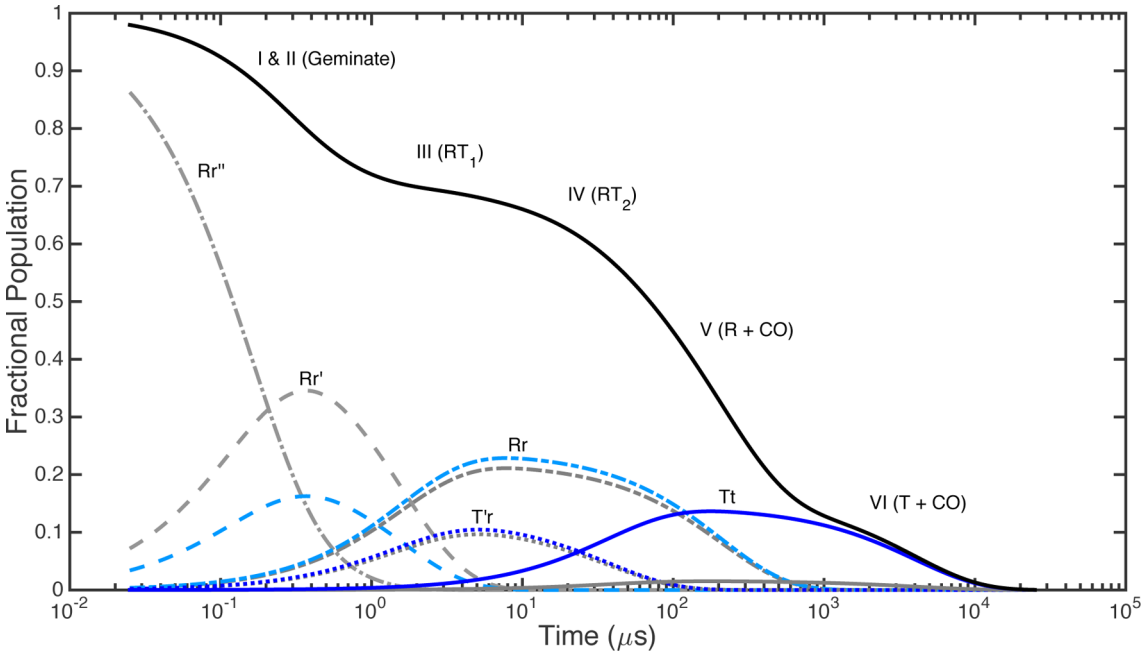

Figure 8. Fractional concentrations of HbCO allosteric intermediates (see Scheme 1), calculated from the data in Tables 2 and 3, illustrate increased heme hydration as protein quaternary/tertiary conformations evolve in time (data for hydrated heme species are colored light and dark blue and data for anhydrous species gray): (gray, –·–) $[Fe\cdots CO]_{Rr''}$, (gray, – – –) $[Fe\cdots]_{Rr'}$, (light blue, – – –) $[Fe\cdots H_2O]_{Rr'}$, (gray, ——) $[Fe\cdots]_{Rr}$, (light blue, ——) $[Fe\cdots H_2O]_{Rr}$, (gray, ···) $[Fe\cdots]_{T'r}$, (dark blue, ···) $[Fe\cdots H_2O]_{T'r}$, (gray, —) $[Fe\cdots]_{Tt}$, and (dark blue, —) $[Fe\cdots H_2O]_{Tt}$. Transition points in the time course of the total fractional population of deoxy hemes (black line) are labeled by the corresponding kinetic phases and their nominal assignments.

b-spectra of random noise, with a magnitude similar to the noise present in the data, produced variations of ≪10% in the Δn_w values. Also, attempts to deconvolute the *b*-spectra with a basis of model spectra that omitted the water entry spectrum produced poor fits (results not shown). The residuals of those fits closely resembled the missing water signal, a finding that supported the uniqueness of the spectral deconvolution results presented here.

To keep the analysis as simple as possible, without compromising the water entry results, we neglected in Scheme 1 any protein structural relaxation occurring on the geminate phase I time scale. As a check on this simplification, we verified that dropping this assumption, and incorporating some arbitrary amount of structural relaxation for phase I into the model, had the effect of modifying only the relaxation amplitude values obtained for the later kinetic phases but had no effect on the Δn_w or Δn_{CO} values obtained from the spectral deconvolution procedure (results not shown). This result provided a further indication of the uniqueness of the Δn_w and Δn_{CO} values obtained from the modeling.

The time evolution of HbCO allosteric intermediates after photodissociation (see Scheme 1), calculated from the time constants and deconvoluted amplitudes in Table 2, is shown in Figure 8. For the sake of simplicity, the two geminate intermediates, distinguished in the phenomenological kinetic modeling by their different observed lifetimes, are plotted together as one species. Data for the distally hydrated forms of the allosteric intermediates are colored light blue (Rr′ and Rr) and dark blue (T′r and Tt), and data for the anhydrous forms are colored gray. The coupling of the allosteric transitions at 2 and 40 μs (labeled RT_1 and RT_2, respectively) to the increased hydration of the Rr, T′r, and Tt intermediate conformations is evident in the figure. The extent of the distal water occupancies for the three hydration equilibria in Scheme 1 is summarized in Table 3, where we take configurations Rr and Tt to represent the equilibrium R and T states, respectively. The water occupancy of the equilibrium R state was higher than would be expected from the average of the isolated subunit occupancies. Similarly, the n_w value of the T state was higher than that expected from the deoxyHb crystal structure.[6] The overall time evolution of n_w for fully unliganded Hb tetramers after CO photolysis, calculated from the time constants and DPW values in Table 2, is shown in Figure 9. After stepwise increases at the geminate rebinding and quaternary structural relaxation phases, bimolecular CO rebinding to the final T state eventually returns n_w to zero.

Table 3. Distal Water Occupancies (n_w), Equilibrium Constants (K_w), and Free Energies of Heme Hydration (ΔG_w) for Species Rr′, Rr, and Tt in Scheme 1

quaternary/tertiary configuration	n_w	K_w	ΔG_w (kJ mol^{-1})
Rr′	0.30	0.43	2.1
Rr	~0.6	1.5	−1.0
Tt	≥0.9	≥9	≤−5.5

DISCUSSION

In the simplest kinetic model, the observed bimolecular ligand rebinding rate constant k' for a heme site is expected to be proportional to three factors: the geminate rebinding yield (ϕ) that represents the fraction of bond formation for ligands in the distal pocket, the rate of diffusion of ligand into an empty heme pocket (k_{in}), and the fraction of water-free empty pockets ($1 - n_w$). Thus, the bimolecular association rate constant is given by[3,19]

DOI: 10.1021/acs.biochem.6b00081
Biochemistry 2016, 55, 4005−4017

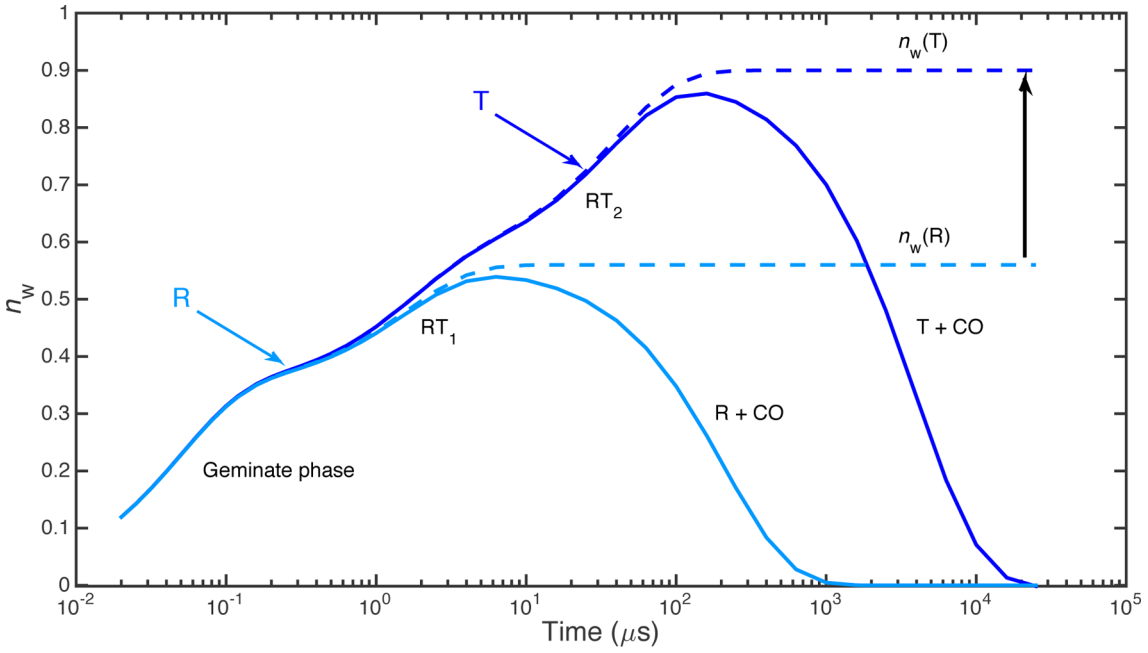

Figure 9. Time evolution of distal pocket water occupancies, n_w, in deoxy hemes of (light blue) R-state and (dark blue) T-state tetramers after CO photolysis, corresponding to the kinetic intermediate shown in Figure 8 (see the text). Dotted lines show asymptotic n_w values for the equilibrium R and T states. The black arrow indicates the increase in heme hydration during the R to T transition.

$$k' = \phi(1 - n_w)k_{in} \quad (2)$$

As a further simplification in applying this expression to the Hb tetramer, we generally neglect differences in these factors between subunits. Although the isolated chains have different geminate yields and bimolecular rebinding rates for O_2 and NO, there is little evidence of large subunit differences in the kinetics of binding of CO to hemoglobin tetramers.[45−48] The experimental results presented here did not directly address subunit differences in DPW occupancy in tetrameric hemoglobin. However, we point out that previous work by Birukou et al. with mutant/native Hb hybrids suggests that in the native R-state tetramer, the α subunits appear to have a water occupancy significantly higher than that of the β subunits,[5] as was also found for the isolated chains. We also assume that the rate of diffusion of ligand through the globin subunits does not depend on the quaternary configuration of the tetramer. Therefore, our attention will focus on the dependencies of the first two factors for k' in eq 2, geminate yield and DPW vacancy, on quaternary state. Finally, eq 2 assumes that heme spectral changes associated with changes in polarity result from water molecules that block access to ligand entry. Some water could also enter the heme pocket in regions that do not directly block movement toward the heme iron atom but still alter its spectral properties. However, there is strong crystallographic evidence that there is water blocking access to the iron atom in the distal pockets of most deoxygenated forms of hemoglobins and myoglobins.[2,6,49]

In previous studies of native and mutant myoglobins and isolated Hb chains, we were able to directly confirm the correlation between distal pocket water occupancies and reductions in CO binding rate constants, and thus the effectiveness of heme hydration in blocking access of ligand to the heme binding site, as factored into eq 2.[8,17,19] However, as discussed below, the quantitative knowledge of the geminate CO rebinding yield that is needed to apply eq 2 to the Hb T state is not available because the yields are so small. Therefore, in evaluating the steric mechanism (Scheme 1) by which distal pocket water modulates access of ligand to heme iron in HbCO allostery, we assume that the presence of a water molecule in the T-state distal pocket is effective in inhibiting ligand molecules from binding to the heme iron atom, as observed in R-state hemoglobin, isolated Hb α chains, and myoglobin.[5,8,19] Knowledge of the ϕ(T)/ϕ(R) ratio for HbCO photolysis would allow us to further test this assumption through eq 2.

Heme Pocket Hydration and Ligand Access. A comparison of the average estimates of n_w for the R and T states, which we rounded to ∼0.6 and ∼0.9, respectively, suggests that changes in heme hydration contribute significantly to the slower ligand recombination rate of the T state relative to that of the R state. The ratio of the R-state bimolecular rate constant to that of the T state was observed to be ∼20 in this study and 30−40 in other studies.[50] The observed bimolecular association rate constant for each state is expected to be proportional to its DPW vacancy factor $(1 - n_w)$.[19] On that basis, the average estimates of n_w for the quaternary states suggest that heme hydration contributed a factor of ∼4 {provided by the factor $[1 - n_w(R)]/[1 - n_w(T)]$} to the observed R/T kinetic ratio. This represents a scenario in which a significant portion of the slowing of the observed CO recombination rate for the T state is due to increased hydration. However, the uncertainties in the water occupancy values (±10%) make such kinetic estimates difficult as the n_w values approach unity. Given those uncertainties, the likely values for the DPW R/T kinetic ratio consistent with the data presented here were spread over a wide range (∼4−20). Thus, it is hard to judge quantitatively how much of the change in k'_{CO} between the R and T states is due to enhanced hydration and how much is due to decreased iron reactivity due to proximal constraints and concomitant decreases in ϕ. However, the conservative estimate of the hydration factor suggested here (∼4) seems to be consistent with previous NO binding

DOI: 10.1021/acs.biochem.6b00081
Biochemistry 2016, 55, 4005−4017

evidence discussed below. In any event, it is clear that distal pocket hydration increases in going from the R state to the T state, which in turn must result in a decrease in the rate of ligand entry.

Distal Pocket Water in DeoxyHb β Subunits. The ≥90% DPW occupancy of the T state, as determined here spectrokinetically, indicates a high water occupancy in both the α and β subunits. This finding was unexpected given that the X-ray crystallographic evidence indicates a near unity occupancy in the α chains, but negligible occupancy in the β chains of the deoxyHb tetramer.[6] The latter situation has been attributed to water exclusion caused by the tighter steric constraints of the β-chain heme pocket. Rather than preventing a water molecule from entering the distal heme pocket, however, the constraint imposed by the smaller distance between the distal histidine residue and the heme plane found in the β chains might merely prevent water that is present from settling into a position that is sufficiently well-ordered for detection in the electron density map. We have observed precedents for this situation in Mb mutants in which steric or electrostatic constraints imposed by heme pocket residues render the distal water molecule too disordered for facile crystallographic detection.[17]

α- and β-Subunit Differences in Tetramer Water Occupancies. The data for distal water entry presented here did not distinguish the water occupancies of α and β chains within the tetramer. Thus, without additional information, the n_w value determined here for the R state, ∼0.6, could reflect equal occupancies for α and β subunits, or near unity occupancy in one subunit type and low occupancy in the other, or some intermediate situation. However, kinetic data from O_2 binding studies by Birukou et al. of R-state E7 mutant−native hybrid hemoglobin tetramers suggest that $n_w(R,\alpha) > n_w(R,\beta)$.[5] Specifically, we used their data to roughly estimate the free energy of heme hydration in α subunits relative to β subunits to be approximately −5 kJ/mol. {Application of eq 1 to the O_2 association rate constants[5] was simplified by assuming small variations in k_{in} between species, and by the fact that geminate recombination yields are roughly near unity for O_2 binding. For each chain type, we compared the average of the rate constants for three apolar E7 mutants assumed to have negligible n_w values (leucine, alanine, and glycine) to that of the native subunit to obtain a value for K_w from eq 1 and the relation $K_w = n_w/(1 - n_w)$. The chain difference in heme hydration free energy was estimated from $-RT \ln[K_w(\alpha)/K_w(\beta)]$.} The differential hydration energy and the subunit-averaged value of n_w determined here, taken together, allowed us to estimate the individual subunit values: $n_w(R,\alpha) = 0.8$, and $n_w(R,\beta) = 0.3$.

The subunit hydration values imply that the additional distal water entry observed upon completion of the R → T transition (Figure 9) occurred mainly in the β subunits. Whereas the α subunits were inferred to have high DPW occupancies in both the R and T states, the β subunits experienced a sharp rise in n_w, from 0.3 to ∼0.9, implying a potentially large increase in steric blockade, even if discrete water molecules cannot be seen in the crystal structures.

α- and β-Subunit Differences in the Allosteric Mechanism. Although the proximal control of heme ligand reactivity through the heme−histidine linkage first proposed by Perutz has tended to dominate discussions of the allosteric mechanism in hemoglobin,[23] it has long been suggested that steric control by distal pocket residues also plays a role.[51] Such a distal mechanism is thought be more important in the β chains than in the α chains, because of chain differences in pocket structure and spectral evidence that the marked changes in proximal histidine−Fe bond tension observed in α chains during the allosteric transition are less evident in the β chains.[52,53] Thus, while the two chain types have very similar affinities in the tetramer, having evolved under selective pressure to maximize cooperativity, they appear to operate through different allosteric mechanisms: a more proximal mechanism in the α chains and a perhaps more distal mechanism in the β chains.[48]

Using the subunit-blind occupancies measured here and independent thermodynamic information,[5] we were able to infer subunit differences in distal water entry during the R → T transition. The chain differences in steric control of ligand binding inferred here were consistent with the subunit differences in allosteric mechanism inferred by previous workers, discussed above. We find the linkage of distal water occupancy to R−T allostery to be stronger in the β chains than in the α chains. This linkage thus appears to offer a structural mechanism for the steric lowering of β-chain ligand association rate constants in the T state that might be related to the previously identified distal mechanism, in which movement of the E helix across the heme face brings the distal histidine, to which water molecules are hydrogen bonded, closer to the ligand binding site, but perhaps in multiple positions because of the closeness of the imidazole ring to the porphyrin ring.

Reactions with NO and Effects of Distal Pocket Water. In principle, eq 2 should also apply to O_2 and NO binding, which show much higher fractions of geminate rebinding due to large rates of internal rebinding to the iron atom. In the case of NO, effectively 100% of the photolyzed ligand recombines on picosecond time scales. As a result, k'_{NO} is thought to represent the bimolecular rate of entry for all diatomic ligands, i.e., $(1 - n_w)k'_{in}$ from eq 2, because $\phi = 1.0$.[5] In 1975, Gibson and Cassoly suggested that k'_{NO} does not change in going from the R state to the T state based on the lack of acceleration of NO binding in rapid mixing experiments and a reported k'_{NO} value equal to 25 μM^{-1} s^{-1} for the first step in binding of NO to presumably T-state HbA.[54] In 2010, Birukou et al. reported that both the isolated and R-state α subunits have a k'_{NO} value of ∼25 μM^{-1} s^{-1}, whereas the k'_{NO} value for R-state β subunits is roughly 70 μM^{-1} s^{-1}.[5] The latter results, combined with Cassoly and Gibson's measurements, suggest that (1) $(1 - n_w)k'_{in}$ is smaller for α subunits than for β subunits in the R state and (2) $(1 - n_w)k'_{in}$ stays the same in α subunits but decreases at least ∼3-fold for β subunits in the T quaternary state. These results are in qualitative agreement with our estimates of n_w in the α and β subunits of both R- and T-state hemoglobin and support the increase in β T-state subunits. It should be noted that similar results are observed for O_2 binding in terms of lower k'_{O_2} values for the R-state α subunit than for β subunits,[5] but in the case of O_2, both the fraction of geminate rebinding and k'_{O_2} decrease significantly in going to the T state, making estimates of rates of entry and n_w difficult.

Comparison with Molecular Dynamics (MD) Simulations. Recent MD simulations of deoxyhemoglobin R- and T-state tetramers suggest that solvent water molecules transiently access the distal heme pockets of the α and β subunits via multiple channels, including the distal histidine gate, on a time scale (0.1−1 μs) consistent with the kinetics observed here.[27] However, variability between simulation runs

DOI: 10.1021/acs.biochem.6b00081
Biochemistry 2016, 55, 4005−4017

in that study prevented a comparison of calculated R-state versus T-state n_w values, and the state-independent n_w values calculated from the simulations were inconsistent with the heme hydration observed in our experiments and crystal structures, e.g., the high DP water occupancy of the α subunits,[6] circumstances that tend to preclude a closer comparison of the MD-calculated heme hydration values with the results presented here. However, these simulations do indicate that water can reach the heme and be located in multiple positions in the distal pocket, a circumstance that could make hydration difficult to observe statically, particularly in β subunits.[27]

CONCLUSIONS

The strong correlation of heme pocket water entry with quaternary structural transitions suggests that water plays a previously unsuspected role in the mechanism of hemoglobin allostery. An increase in distal heme pocket water occupancy during the R to T quaternary transition can account in part for a significant lowering of ligand association rate constants, particularly in β subunits. After photolysis, hydration of unliganded heme pockets proceeds over several kinetic steps, which are tied to protein tertiary and quaternary structural relaxation. The net result is higher distal water occupancy in the T-state tetramer than would be expected from the distal pocket water occupancies of the isolated chains. This increased water displacement barrier in the T state appears to act in concert with out-of-plane movement of the heme iron to reduce the bimolecular rates of all diatomic ligands. Thus, allosteric changes in protein tertiary structure near the heme, which on the proximal side pull the iron atom out of the porphyrin plane and dome the heme moiety, appear to also extend to tertiary changes on the distal side that better accommodate water in the T state. The increase in distal histidine−water hydrogen bonding appears to contribute significantly to the forces driving the R to T transition and to the decrease in ligand affinity.

AUTHOR INFORMATION

Corresponding Authors

*Department of Chemistry and Biochemistry, University of California, Santa Cruz, 1156 High St., Santa Cruz, CA 95064. E-mail: goldbeck@ucsc.edu. Telephone: (831) 459-4007. Fax: (831) 459-2935.

*Department of Chemistry and Biochemistry, San Francisco State University, 1600 Holloway Ave., San Francisco, CA 94132. E-mail: esquerra@sfsu.edu. Telephone: (415) 338-1288. Fax: (415) 338-2384.

Present Address

‖I.B.: Syngenta, Research Triangle Park, NC 27709.

Funding

This work was supported financially by National Institutes of Health (NIH) Grants 5SC3GM103748 (R.M.E.), HL110900 (J.S.O.), and GM035649 (J.S.O.); Robert A. Welch Grant C-0612 (J.S.O.); and a student fellowship from NIH Grant GM008574 (Minority Access to Research Careers) (B.M.B.).

Notes

The authors declare no competing financial interest.

ABBREVIATIONS

DPW, distal pocket water; SVD, singular value decomposition; TROA, time-resolved optical absorption.

REFERENCES

(1) Phillips, G. N., and Pettitt, B. M. (1995) Structure and dynamics of the water around myoglobin. *Protein Sci. 4*, 149−158.

(2) Quillin, M. L., Arduini, R. M., Olson, J. S., and Phillips, G. N., Jr. (1993) High-resolution crystal structures of distal histidine mutants of sperm whale myoglobin. *J. Mol. Biol. 234*, 140−155.

(3) Olson, J. S., and Phillips, G. N., Jr. (1997) Myoglobin discriminates between O_2, NO, and CO by electrostatic interactions with the bound ligand. *JBIC, J. Biol. Inorg. Chem. 2*, 544−552.

(4) Tsai, A. L., Berka, V., Martin, E., and Olson, J. S. (2012) A "sliding scale rule" for selectivity among NO, CO, and O_2 by heme protein sensors. *Biochemistry 51*, 172−186.

(5) Birukou, I., Schweers, R. L., and Olson, J. S. (2010) Distal histidine stabilizes bound O2 and acts as a gate for ligand entry in both subunits of adult human hemoglobin. *J. Biol. Chem. 285*, 8840−8854.

(6) Fermi, G., Perutz, M. F., Shaanan, B., and Fourme, R. (1984) The crystal structure of human deoxyhemoglobin at 1.74 Å resolution. *J. Mol. Biol. 175*, 159−174.

(7) Mathews, A. J., Rohlfs, R. J., Olson, J. S., Tame, J., Renaud, J. P., and Nagai, K. (1989) The effects of E7 and E11 mutations on the kinetics of ligand binding to R state human hemoglobin. *J. Biol. Chem. 264*, 16573−16583.

(8) Esquerra, R. M., Lopez-Pena, I., Tipgunlakant, P., Birukou, I., Nguyen, R. L., Soman, J., Olson, J. S., Kliger, D. S., and Goldbeck, R. A. (2010) Kinetic spectroscopy of heme hydration and ligand binding in myoglobin and isolated hemoglobin chains: an optical window into heme pocket water dynamics. *Phys. Chem. Chem. Phys. 12*, 10270−10278.

(9) Bonaventura, C., Bonaventura, J., Shih, D. T., Iben, E. T., and Friedman, J. (1999) Altered ligand rebinding kinetics due to distal-side effects in hemoglobin Chico ($Lys^{\beta 66}$(E10) → Thr. *J. Biol. Chem. 274*, 8686−8693.

(10) Ouellet, Y. H., Daigle, R., Lague, P., Dantsker, D., Milani, M., Bolognesi, M., Friedman, J. M., and Guertin, M. (2008) Ligand binding to truncated hemoglobin N from Mycobacterium tuberculosis is strongly modulated by the interplay between the distal heme pocket residues and internal water. *J. Biol. Chem. 283*, 27270−27278.

(11) Bustamante, J. P., Abbruzzetti, S., Marcelli, A., Gauto, D., Boechi, L., Bonamore, A., Boffi, A., Bruno, S., Feis, A., Foggi, P., Estrin, D. A., and Viappiani, C. (2014) Ligand uptake modulation by internal water molecules and hydrophobic cavities in hemoglobins. *J. Phys. Chem. B 118*, 1234−1245.

(12) Williams, M. A., Goodfellow, J. M., and Thornton, J. M. (1994) Buried waters and internal cavities in monomeric proteins. *Protein Sci. 3*, 1224−1235.

(13) Halle, B. (1998) Water in biological systems: The NMR picture. In *Hydration Processes in Biology* (Bellisent-Funel, M.-C., Ed.) pp 233−249, IOS Press, Dordrecht, The Netherlands.

(14) Zhang, X. J., and Matthews, B. W. (1994) Conservation of solvent-binding sites in 10 crystal forms of T4 lysozyme. *Protein Sci. 3*, 1031−1039.

(15) Denisov, V. P., and Halle, B. (1994) Dynamics of the internal and external hydration of globular proteins. *J. Am. Chem. Soc. 116*, 10324−10325.

(16) Imai, T., Hiraoka, R., Kovalenko, A., and Hirata, F. (2007) Locating missing water molecules in protein cavities by the three-dimensional reference interaction site model theory of molecular solvation. *Proteins: Struct., Funct., Genet. 66*, 804−813.

(17) Goldbeck, R. A., Pillsbury, M. L., Jensen, R. A., Mendoza, J. L., Nguyen, R. L., Olson, J. S., Soman, J., Kliger, D. S., and Esquerra, R. M. (2009) Optical detection of disordered water within a protein cavity. *J. Am. Chem. Soc. 131*, 12265−12272.

(18) Damjanovic, A., Schlessman, J. L., Fitch, C. A., Garcia, A. E., and Garcia-Moreno E, B. (2007) Role of flexibility and polarity as determinants of the hydration of internal cavities and pockets in proteins. *Biophys. J. 93*, 2791−2804.

(19) Goldbeck, R. A., Bhaskaran, S., Ortega, C., Mendoza, J. L., Olson, J. S., Soman, J., Kliger, D. S., and Esquerra, R. M. (2006) Water and ligand entry in myoglobin: Assessing the speed and extent of heme

DOI: 10.1021/acs.biochem.6b00081
Biochemistry 2016, 55, 4005−4017

pocket hydration after CO photodissociation. *Proc. Natl. Acad. Sci. U. S. A. 103*, 1254−1259.
(20) Esquerra, R. M., Jensen, R. A., Bhaskaran, S., Pillsbury, M. L., Mendoza, J. L., Lintner, B. W., Kliger, D. S., and Goldbeck, R. A. (2008) The pH dependence of heme pocket hydration and ligand rebinding kinetics in photodissociated carbonmonoxymyoglobin. *J. Biol. Chem. 283*, 14165−14175.
(21) Schotte, F., Soman, J., Olson, J. S., Wulff, M., and Anfinrud, P. A. (2004) Picosecond time-resolved X-ray crystallography: Probing protein function in real time. *J. Struct. Biol. 147*, 235−246.
(22) Monod, J., Wyman, J., and Changeux, J. P. (1965) On the nature of allosteric transitions: A plausible model. *J. Mol. Biol. 12*, 88−118.
(23) Perutz, M. F. (1970) Stereochemistry of cooperative effects in haemoglobin. *Nature 228*, 726−739.
(24) Szabo, A., and Karplus, M. (1972) A mathematical model for structure-function relations in hemoglobin. *J. Mol. Biol. 72*, 163−197.
(25) Colombo, M. F., Rau, D. C., and Parsegian, V. A. (1992) Protein solvation in allosteric regulation: A water effect on hemoglobin. *Science 256*, 655−659.
(26) Goldbeck, R. A., Paquette, S. J., and Kliger, D. S. (2001) The effect of water on the rate of conformational change in protein allostery. *Biophys. J. 81*, 2919−2934.
(27) Shadrina, M. S., Peslherbe, G. H., and English, A. M. (2015) O_2 and water migration pathways between the solvent and heme pockets of hemoglobin with open and closed conformations of the distal HisE7. *Biochemistry 54*, 5279−5289.
(28) Parkhurst, K. M., and Parkhurst, L. J. (1992) Rapid preparation of native alpha and beta chains of human hemoglobin. *Int. J. Biochem. 24*, 993−998.
(29) Goldbeck, R. A., Esquerra, R. M., Holt, J. M., Ackers, G. K., and Kliger, D. S. (2004) The molecular code for hemoglobin allostery revealed by linking the thermodynamics and kinetics of quaternary structural change. 1. Microstate linear free energy relations. *Biochemistry 43*, 12048−12064.
(30) Henry, E. R., and Hofrichter, J. (1992) Singular value decomposition: Application to analysis of experimental data. *Methods Enzymol. 210*, 129−192.
(31) Goldbeck, R. A., and Kliger, D. S. (2001) Transient kinetic studies. In *Encyclopedia of Chemical Physics and Physical Chemistry* (Moore, J. H., and Spencer, N. D., Eds.) pp 2637−2656, IOP, Bristol, U.K.
(32) Szundi, I., Lewis, J. W., and Kliger, D. S. (1997) Deriving reaction mechanisms from kinetic spectroscopy. Application to late rhodopsin intermediates. *Biophys. J. 73*, 688−702.
(33) Cao, W., Christian, J. F., Champion, P. M., Rosca, F., and Sage, J. T. (2001) Water penetration and binding to ferric myoglobin. *Biochemistry 40*, 5728−5737.
(34) Lindqvist, L., El Mohsni, S., Tfibel, F., and Alpert, B. (1980) Transient haem-globin interactions in photodeligated carboxyhaemoglobin and subunits. *Nature 288*, 729−730.
(35) Brunori, M., Antonini, E., Wyman, J., and Anderson, S. R. (1968) Spectral differences between haemoglobin and isolated haemoglobin chains in the deoxygenated state. *J. Mol. Biol. 34*, 357−359.
(36) Perutz, M. F., Fersht, A. R., Simon, S. R., and Roberts, G. C. (1974) Influence of globin structure on the state of the heme. II. Allosteric transitions in methemoglobin. *Biochemistry 13*, 2174−2186.
(37) Goldbeck, R. A., Paquette, S. J., Bjorling, S. C., and Kliger, D. S. (1996) Allosteric intermediates in hemoglobin. 2. Kinetic modeling of HbCO photolysis. *Biochemistry 35*, 8628−8639.
(38) Goldbeck, R. A., Esquerra, R. M., Kliger, D. S., Holt, J. M., and Ackers, G. K. (2004) The molecular code for hemoglobin allostery revealed by linking the thermodynamics and kinetics of quaternary structural change. 2. Cooperative free energies of $(\alpha(\mathrm{FeCO})\beta(\mathrm{Fe}))_2$ and $(\alpha(\mathrm{Fe})\beta(\mathrm{FeCO}))_2$ T-state tetramers. *Biochemistry 43*, 12065−12080.
(39) Esquerra, R. M., Goldbeck, R. A., Reaney, S. H., Batchelder, A. M., Wen, Y., Lewis, J. W., and Kliger, D. S. (2000) Multiple geminate ligand recombinations in human hemoglobin. *Biophys. J. 78*, 3227−3239.
(40) Goldbeck, R. A., Esquerra, R. M., and Kliger, D. S. (2002) Hydrogen bonding to Trp β37 is the first step in a compound pathway for hemoglobin allostery. *J. Am. Chem. Soc. 124*, 7646−7647.
(41) Bjorling, S. C., Goldbeck, R. A., Paquette, S. J., Milder, S. J., and Kliger, D. S. (1996) Allosteric intermediates in hemoglobin. 1. Nanosecond time-resolved circular dichroism spectroscopy. *Biochemistry 35*, 8619−8627.
(42) Balakrishnan, G., Case, M. A., Pevsner, A., Zhao, X., Tengroth, C., McLendon, G. L., and Spiro, T. G. (2004) Time-resolved absorption and UV resonance Raman spectra reveal stepwise formation of T quaternary contacts in the allosteric pathway of hemoglobin. *J. Mol. Biol. 340*, 843−856.
(43) Fischer, S., Olsen, K. W., Nam, K., and Karplus, M. (2011) Unsuspected pathway of the allosteric transition in hemoglobin. *Proc. Natl. Acad. Sci. U. S. A. 108*, 5608−5613.
(44) Cammarata, M., Levantino, M., Wulff, M., and Cupane, A. (2010) Unveiling the timescale of the R-T transition in human hemoglobin. *J. Mol. Biol. 400*, 951−962.
(45) Henry, E. R., Jones, C. M., Hofrichter, J., and Eaton, W. A. (1997) Can a two-state MWC allosteric model explain hemoglobin kinetics? *Biochemistry 36*, 6511−6528.
(46) Hofrichter, J., Henry, E. R., Sommer, J. H., Deutsch, R., Ikeda-Saito, M., Yonetani, T., and Eaton, W. A. (1985) Nanosecond optical spectra of iron-cobalt hybrid hemoglobins: geminate recombination, conformational changes, and intersubunit communication. *Biochemistry 24*, 2667−2679.
(47) Bandyopadhyay, D., Magde, D., Traylor, T. G., and Sharma, V. S. (1992) Quaternary structure and geminate recombination in hemoglobin: flow-flash studies on $\alpha_2^{CO}\beta_2$ and $\alpha_2\beta_2^{CO}$. *Biophys. J. 63*, 673−681.
(48) Unzai, S., Eich, R., Shibayama, N., Olson, J. S., and Morimoto, H. (1998) Rate constants for O_2 and CO binding to the α and β subunits within the R and T states of human hemoglobin. *J. Biol. Chem. 273*, 23150−23159.
(49) Phillips, S. E. (1980) Structure and refinement of oxymyoglobin at 1.6 Å resolution. *J. Mol. Biol. 142*, 531−554.
(50) Olson, J. S., Foley, E. W., Maillett, D. H., and Paster, E. V. (2003) Measurement of rate constants for reactions of O_2, CO, and NO with hemoglobin. *Methods Mol. Med. 82*, 65−91.
(51) Perutz, M. F. (1990) *Mechanisms of Cooperativity and Allosteric Regulation in Proteins*, Cambridge University Press, Cambridge, England.
(52) Balakrishnan, G., Ibrahim, M., Mak, P. J., Hata, J., Kincaid, J. R., and Spiro, T. G. (2009) Linking conformation change to hemoglobin activation via chain-selective time-resolved resonance Raman spectroscopy of protoheme/mesoheme hybrids. *JBIC, J. Biol. Inorg. Chem. 14*, 741−750.
(53) Jones, E. M., Monza, E., Balakrishnan, G., Blouin, G. C., Mak, P. J., Zhu, Q. H., Kincaid, J. R., Guallar, V., and Spiro, T. G. (2014) Differential control of heme reactivity in alpha and beta subunits of hemoglobin: A combined Raman spectroscopic and computational study. *J. Am. Chem. Soc. 136*, 10325−10339.
(54) Cassoly, R., and Gibson, Q. (1975) Conformation, co-operativity and ligand binding in human hemoglobin. *J. Mol. Biol. 91*, 301−313.

DOI: 10.1021/acs.biochem.6b00081
Biochemistry 2016, 55, 4005−4017